PHYSICAL REVIEW A VOLUME 36, NUMBER 6 SEPTEMBER 15, 1987

Two-electron excitations in atomic calcium. I

Chris H. Greene and Longhuan Kim
Department of Physics and Astronomy, Louisiana State University, Baton Rouge, Louisiana 70803
(Received 26 March 1987)

The pattern of electron correlations is examined for odd-parity $L=1$ states of calcium over a wide range of energies from far below the $4s$ threshold up to the $4p$ threshold of Ca^+. By combining quantum-defect theory with a small-scale eigenchannel R-matrix calculation, good agreement with the observed photoabsorption spectrum is obtained. The two-electron probability densities and channel-interaction parameters are analyzed as functions of the total energy. A novel interference between direct ($4s\varepsilon p$-$3d\varepsilon p$) and indirect ($4s\varepsilon p$-$4p\varepsilon s$-$3d\varepsilon p$) channel-interaction amplitudes greatly reduces the width of the $3d6p$ autoionizing resonance compared to adjacent series members.

I. INTRODUCTION

The calcium photoabsorption spectrum up to 10 eV has proved unexpectedly difficult to describe theoretically.[1,2] We show in this paper that a reformulated version[3,4] of the eigenchannel R-matrix method[5] when combined with multichannel quantum-defect theory (MQDT) (Refs. 6–8) successfully describes most features of the observed spectrum.[9–12] This calculation requires somewhat more sophistication than the corresponding treatment of beryllium or magnesium[13–15] for two main reasons. First, the effective $l=2$ independent-electron potential is just slightly too shallow to support a short-range $3d$ bound state.[16] In contrast to Be and Mg, the simplest independent-electron models such as the Hartree-Slater model cannot provide a sufficiently accurate description of the e-Ca^{2+} interaction. A second complication posed by calcium and the heavier alkaline-earth metals stems from the smaller binding energy of the "one-electron" ion Ca^+. Virtual excitations into higher "strongly closed" channels such as $5snp$ and $4dnp$ therefore play a much stronger role than in Be and Mg, where they have usually been neglected entirely. Angular correlations between the two valence electrons are also much stronger in Ca, since the $Ca^+(3d)$ level lies only 0.06 a.u. above the $Ca^+(4s)$ ground state. Because of these complications, we have attempted to be more systematic than Ref. 15 in determining which independent-electron trial functions are most important for obtaining accurately converged wave functions and photoionization cross sections.

We also examine the mechanisms underlying the unusually strong channel interactions in all of the alkaline-earth atoms. This is accomplished by plotting the primitive mixing parameters of MQDT as functions of energy, and by displaying the radial probability densities. These show how new channels "turn on" as the energy is increased. They also show how direct and indirect autoionization pathways interfere, causing the net $4s\varepsilon p$-$3d\varepsilon p$ ($^1P^o$) interaction strength to vanish at an energy close to the $3d6p$ autoionizing level.

Our treatment shares many similarities with the recent R-matrix study of doubly excited strontium by Aymar *et al.*,[17] which also finds good agreement with observed spectra. Reference 17 confirms for the strontium atom most of our conclusions about the major theoretical elements required to describe calcium realistically.

In recent years the growth of multiphoton laser spectroscopy has sparked numerous experimental investigations of doubly excited alkaline-earth atoms.[18–22] Most of these have dealt with barium, whose spectrum is complicated by a severe breakdown of LS coupling resulting from the strong spin-orbit interaction. For such experiments the only available type of theoretical analysis uses empirical MQDT mixing parameters which are adjusted to agree with a particular set of measurements. The number of parameters can be quite large;[23] the $J=1$, odd-parity states of barium for instance, have been characterized by an eight-channel fit involving 21 empirical parameters.[24,25] Accurate channel-mixing parameters are useful for describing Rydberg spectra of free atoms as well as those distorted by the presence of an external electric[26] or magnetic[27] field, or by rare-gas-perturbing atoms.[28] This makes it desirable to develop improved techniques to predict these mixing parameters, particularly when they depend strongly on the energy.

Two previous studies of calcium in the same energy range considered in this paper should be mentioned. The first was a many-body perturbation theory (MBPT) calculation performed by Altun *et al.*[1] The MBPT results did a surprisingly good job of describing the global oscillator-strength distribution, considering the fact that channel interactions are so strong. Still, its agreement with experiment deteriorates rapidly as the energy increases toward the $3d$ threshold, and shows very little resemblance to experiment above this threshold. The larger-scale R-matrix calculation of Scott *et al.*[2] should have been capable of dealing with the strong electron correlations and channel mixing, but below the $3d$ threshold it shows larger departures from experiment than the MBPT results. Between the $3d$ and $4p$ thresholds their R-matrix treatment gives a distinct improvement, although its self-consistency remains rather poor (as manifested by length and velocity results for the

cross section which often differ by a factor of 2).[2] It is worth pointing out that reasonably good results were obtained instead for barium, ostensibly a much more complicated atom than Ca, by an R-matrix calculation[29] which used a model potential and included relativistic terms in the Hamiltonian.

We adopt in this study a reformulation[3,4] of the R-matrix method that has proved to be simple, reliable, and rapidly convergent in calculations of $^1P^o$ and $^1D^e$ states[15,30] of Be and Mg, and of $^2D^e$ states of Al.[31] This reformulation uses a variational expression for the eigenvalues of the R matrix, i.e., for the (negative of the) normal logarithmic derivative on the surface of the finite reaction volume. When a linear combination of nonorthogonal Slater-determinantal orbitals is used as a trial function in the variational functional, good convergence is achieved with modest-size basis sets. In contrast to Refs. 2, 29, and 32, no "Buttle correction" to the resulting R matrix is needed to correct for nonuniform convergence problems. Despite its being a close relative of the Kohn variational principle[33] it does not appear to suffer from any problematic Kohn-type anomalies.[34,35] By matching to a channel expansion involving Coulomb wave functions at the surface ($r=r_0$) of the reaction volume, the channel-mixing parameters of MQDT (elements of the short-range reaction matrix) are found directly as explicit slowly varying functions of energy. The calculation of any desired observables can then be performed rapidly on a fine energy mesh, giving discrete energy levels and oscillator strengths, total and partial photoionization cross sections, and anisotropy parameters such as the photoelectron angular distribution asymmetry and spin polarization or the alignment and orientation of the ionic residue.[6–8,36]

II. THEORETICAL DESCRIPTION OF THE HEAVY ALKALINE-EARTH ATOMS

A. The one-electron Hamiltonian

Alkaline-earth spectra can be adequately described up to and somewhat beyond the two-electron ionization threshold by a Hamiltonian having the basic structure (in a.u.)

$$H=h(\mathbf{r}_1)+h(\mathbf{r}_2)+1/r_{12} \ . \tag{1}$$

The effective one-electron Hamiltonian $h(\mathbf{r})$ includes the electron kinetic energy $-\frac{1}{2}\nabla^2$ and a radial l-dependent potential $v_l(r)$ which describes mainly the net screened nuclear potential experienced by a valence electron. The nonvalence core electrons can be assumed to be frozen in their respective one-electron orbitals and will be ignored except to the extent that they determine $v_l(r)$. In previous studies of Be and Mg,[15,30] an l-independent Hartree-Slater potential $v(r)$ was used to describe the e-Be^{2+} and e-Mg^{2+} interactions. For calcium and the heavier alkaline-earth metals more sophistication is needed, as is clear from the large ($\sim 10\%$) errors in Hartree-Slater binding energies of the outermost electron in Ca^+. Calcium poses particular difficulties in this regard, since its close proximity to scandium makes the d-wave potential unusually sensitive. (Scandium is, of course, the first atom with a d electron in its ground-state configuration.) Since our present interests concern the description of correlated two-electron motion, we have *not* attempted to find a highly accurate *ab initio* description of Ca^+. Instead we make a small empirical polarization correction to a set of Hartree-Slater potentials $v_l(r)$ chosen such that the one-electron s, p, and d levels of Ca^+ are accurately reproduced.

The form of the e-Ca^{2+} potential used is similar to the e-Ba^{2+} potential of Bartschat, Rudge, and Scott.[29] It includes a screening term and an empirical core polarization term with a cutoff,

$$v_l(r)=v_l^{\mathrm{HS}}(r)-\frac{\alpha_{\mathrm{CP}}}{2r^4}\{1-\exp[-(r/r_{cl})^6]\} \ . \tag{2}$$

The screening term $v_l^{\mathrm{HS}}(r)$ is obtained from a standard Hartree-Slater program[37] which is run separately for the $4s$, $4p$, and $3d$ orbitals of Ca^+. The Kohn-Sham value ($\frac{2}{3}$) is used for the coefficient of the exchange-energy term.[38] The self-energy of the valence electron is subtracted from the Ca^+ potential by using the Latter correction during the iteration of the Hartree-Slater calculation. The core polarization α_{CP} and the l-dependent "cutoff radius" r_{cl} are then adjusted crudely to give optimum agreement with the known spectrum of Ca^+. The final values obtained are $\alpha_{cp}=8.0$, $r_{c0}=1.109$,

TABLE I. Energy levels of Ca^+.

States	E (observed) (a.u.)	E (calculated) (a.u.)
$4s$	−0.436 26	−0.436 27
$5s$	−0.198 57	−0.198 82
$6s$	−0.114 23	−0.114 35
$7s$	−0.074 26	−0.074 34
$8s$	−0.052 15	−0.052 21
$9s$		−0.038 68
$10s$		−0.029 80
$4p$	−0.320 80	−0.320 80
$5p$	−0.160 20	−0.160 19
$6p$	−0.096 77	−0.096 76
$7p$		−0.064 87
$8p$		−0.046 52
$9p$		−0.035 01
$10p$		−0.027 30
$3d$	−0.373 90	−0.373 89
$4d$	−0.177 23	−0.181 77
$5d$	−0.104 89	−0.107 11
$6d$	−0.069 36	−0.070 58
$7d$	−0.049 26	−0.050 01
$8d$	−0.036 78	−0.037 28
$9d$		−0.028 86
$4f$	−0.126 19	−0.127 12
$5f$	−0.080 73	−0.081 21
$6f$	−0.056 01	−0.056 28
$7f$	−0.041 12	−0.041 13
$8f$	−0.031 29	−0.031 56
$9f$	−0.024 84	−0.024 89
$10f$	−0.020 11	−0.020 01

$r_{c1}=1.420$, and for $l\geq 2$, $r_{cl}=1.089$. Table I compares the final calculated one-electron energy levels to the observed levels.[39] While the final e-Ca^{2+} potentials $V_l(r)$ are in a sense "empirical," we emphasize that they have been optimized to agree with known properties of Ca^+ only, and *not* on the basis of our final calculations for neutral calcium.

B. Variational calculation of R-matrix eigenstates

The noniterative reformulation of the eigenchannel R-matrix method used in the present study has been discussed in detail elsewhere.[3,4,15] Here we only summarize its major elements. The most important conceptual element, as in all R-matrix treatments, is the restriction of the nontrivial part of the calculation to a finite (reaction) volume V in configuration space. The "R-matrix eigenenchannels" ψ_β are those eigenstates of the Hamiltonian at any desired energy E whose negative logarithmic derivatives b_β are constant over the surface S enclosing the reaction volume.[5] When the variational trial function is a linear combination of known (real) functions y_k, $\psi=\sum_k c_k y_k$, then the stationary value of b_β is an eigenvalue of a generalized linear eigensystem,

$$\underline{\Gamma}\mathbf{C}=b\underline{\Lambda}\mathbf{C}\ , \tag{3}$$

where

$$\Gamma_{kk'}=2\int_V y_k(E-H)y_{k'}dv-\int_S y_k\frac{\partial y_{k'}}{\partial n}ds \tag{4}$$

and where

$$\Lambda_{kk'}=\int_S y_k y_{k'}ds\ . \tag{5}$$

Solution of this eigensystem determines the phase and amplitude information on the reaction surface that is needed to obtain ψ_β outside the volume V using a multichannel quantum-defect expansion.

The selection of a sensible basis set is important here, as in any variational treatment. We use the simplest such basis consisting of antisymmetrized products of one-electron orbitals $u_{nl}(r)Y_{lm}(\Omega)$, eigenfunctions of $h(\mathbf{r})$ in Eq. (1),

$$-\frac{1}{2}\frac{d^2}{dr^2}u_{nl}(r)+\left[\frac{l(l+1)}{2r^2}+v_l(r)-E_{nl}\right]u_{nl}(r)=0\ . \tag{6}$$

[Note that we work with rescaled wave functions $\psi=r_1r_2\Psi$ throughout this paper in order to eliminate first-derivative terms in the Hamiltonian. Then $b_\beta\equiv-\partial(\ln\psi_\beta)/\partial r\,|_{r=r_0}$.] It will be convenient to distinguish two types of one-electron radial eigenfunctions in Eq. (6), depending on their values at the reaction surface $r=r_0$. The "closed type," denoted $u^c_{nl}(r)$, vanishes at $r=r_0$, while the "open type," denoted $u^o_{nl}(r)$ does not vanish at r_0. When a particular channel is *forced* to be strongly closed at the outset of the calculation, only the closed type of radial functions are included for that channel in the variational basis set. For an open or weakly closed channel, orbitals of each type are included. In practice the solutions $u^c_{nl}(r)$ are calculated numerically first, determining each eigenfunction and its corresponding eigenenergy E^c_{nl}. This basis would be complete if all such states were included, but in order to represent a general continuum function ψ_β which does not generally vanish at r_0, this basis is augmented by a small number of functions $u^o_{nl}(r)$ in each open or weakly closed channel. In our experience good convergence is usually achieved using about seven functions of the type u^c_{nl} in each such channel, and two or three of the type u^o_{nl}. The latter are obtained by solving Eq. (6) at energies E^0_{nl} midway between successive eigenvalues E^c_{nl} and $E^c_{n+1,l}$. The radial functions $u^c_{nl}(r)$ are thus orthonormal over the range $0\leq r\leq r_0$, but the $u^o_{nl}(r)$ are not. One difference compared to previous calculations with this method is that, for instance, Ref. 15 uses a different potential to determine e-Be^{2+} bound functions than is used to represent the e-Be^+ continuum orbitals. This may speed convergence of the R-matrix calculation slightly, but for two-electron atoms, at least, the convergence is so rapid that the extra bother is unnecessary.

The spatial part of each antisymmetric LS-coupled two-electron basis function y_k is expressed in terms of one-electron orbitals by

$$\begin{aligned}y_{n_1l_1n_2l_2}&=2^{-1/2}[u_{n_1l_1}(r_1)u_{n_2l_2}(r_2)Y_{l_1l_2LM}(\Omega_1,\Omega_2)\\&\quad+(-1)^{l_1+l_2-L+S}u_{n_2l_2}(r_1)u_{n_1l_1}(r_2)\\&\quad\times Y_{l_2l_1LM}(\Omega_1,\Omega_2)]\ .\end{aligned} \tag{7}$$

An alternative form for Eq. (7) connects more naturally to the quantum-defect description of the outer region

$$\begin{aligned}y_{in_2}&=2^{-1/2}[\phi_i(r_1;\Omega_1,\Omega_2)u_{n_2l_2}(r_2)\\&\quad+(-1)^S\phi_i(r_2;\Omega_2,\Omega_1)u_{n_2l_2}(r_1)]\ ,\end{aligned} \tag{8}$$

where $i\equiv\{n_1l_1l_2\}$, and where

$$\phi_i(r;\Omega_1,\Omega_2)\equiv u^c_{n_1l_1}(r)Y_{l_1l_2LM}(\Omega_1,\Omega_2)\ . \tag{9}$$

The superscript c in Eq. (9) indicates that the surface harmonic[3] ϕ_i vanishes at $r_1=r_0$. Because we assume that both valence electrons cannot simultaneously escape the reaction zone in the energy range studied here, at least one of the two radial orbitals in Eq. (7) should be of the closed type. On the other hand, the set $u_{n_2l_2}(r_2)$ in Eqs. (8) and (9) generally includes both types of orbitals c and o which, respectively, vanish and do not vanish at r_0.

Numerical calculation of the matrix elements of $\underline{\Gamma}$ and $\underline{\Lambda}$ in Eqs. (4) and (5) is reasonably straightforward. Standard CI programs[40] could be used, in principle, after truncating all integrals to the finite range $r<r_0$. For the two-electron problem studied presently, these integrals are easily obtained and no published computer codes have been used. Matrix elements of the one-electron Hamiltonian h become trivial since the basis functions (7) are eigenfunctions of $h(\mathbf{r}_1)+h(\mathbf{r}_2)$. Instead the evaluation of $1/r_{12}$ matrix elements is more time consuming, but it can be performed once and for all since our basis set is energy independent. The surface integrals in Eqs. (4) and (5) are somewhat less standard. Each element of Eq. (5), for example, has the following form:

$$\Lambda_{n_1 l_1 n_2 l_2, n_1' l_1' n_2' l_2'} = \delta_{l_1 l_1'} \delta_{l_2 l_2'} [O^{(l_1)}_{n_1 n_1'} u_{n_2 l_2} u_{n_2' l_2'} + O^{(l_2)}_{n_2 n_2'} u_{n_1 l_1} u_{n_1' l_1'}] + (-1)^{l_1 + l_2 - L + S} \delta_{l_1 l_2'} \delta_{l_2 l_1'} [O^{(l_2)}_{n_2 n_1'} u_{n_1 l_1} u_{n_2' l_2'} + O^{(l_1)}_{n_1 n_2'} u_{n_2 l_2} u_{n_1' l_1'}] , \tag{10}$$

where the one-electron radial overlap integral is given by

$$O^{(l)}_{nn'} = \int_0^{r_0} u_{nl}(r) u_{n'l'}(r) dr . \tag{11}$$

In Eq. (10) u_{nl} is an abbreviation for $u_{nl}(r_0)$. A second surface term required in Eq. (4) can be obtained by replacing each "primed" $u_{n'l'}$ in Eq. (10) by its radial derivative evaluated at $r = r_0$.

In trial calculations performed to study convergence, we included anywhere from 40 to 128 two-electron basis functions. Table II shows the final basis sets used. The number of channels retained in the R-matrix calculation is dictated by the energy range to be treated and by the size of the reaction volume. By this "number of channels" we mean specifically the number of open or weakly closed channels in which the outermost electron can escape beyond $r = r_0$. All such channels require at least one trial function of the type $u^o_{n_2 l_2}(r)$ which is nonzero at $r = r_0$. Trial functions associated with strongly closed channels, such as $5s5p$, can make an important contribution to the variational calculation, especially in the heavier alkaline-earth metals but also at high energies in any atom. The physical importance of such functions presumably stems mostly from their role in describing the polarization distortion of one-electron ionic wave functions induced by the presence of the second electron. Alternatively, the use of polarized orbitals as in Ref. 17 might adequately account for this distortion in many problems, and permit a somewhat smaller basis set.

C. Energy-dependent MQDT parameters

The variational wave function ψ_β associated with the eigenvalue b_β of Eq. (3) can be expanded in the following form on the reaction surface:

$$\psi_\beta = 2^{-1/2} \sum_{i=1}^{N} [\phi_i(r_1; \Omega_1, \Omega_2) + (-1)^S \phi_i(r_2; \Omega_2, \Omega_1)] F_{i\beta}(r_0), \quad \text{on } S \tag{12}$$

where N is the number of open or weakly closed channels as defined in Sec. II B. The elements of $F_{i\beta}(r_0)$ are easily evaluated in terms of the eigenvector $c_{k\beta}$ of Eq. (3). The normal derivative of ψ_β on the surface S is simply Eq. (12) multiplied by $-b_\beta$. Because the e-Ca^+ potential is Coulombic at $r \geq r_0$, the form (12) is retained beyond the reaction volume as well, with $F_{i\beta}(r_0)$ a linear combination of energy-normalized regular and irregular Coulomb functions (f_i, g_i) in channel i,

$$F_{i\beta}(r) = f_i(r) I_{i\beta} - g_i(r) J_{i\beta}, \quad r \geq r_0 . \tag{13}$$

The Coulomb functions (having Wronskian $2/\pi$) are evaluated[41] at the photoelectron energy $\varepsilon_i = E - E_i$ and for the photoelectron angular momentum appropriate in channel i. The coefficients $I_{i\beta}$ and $J_{i\beta}$ are then just

$$I_{I\beta} = \frac{\pi}{2} F_{i\beta}(r_0)[g_i'(r_0) + b_\beta g_i(r_0)] ,$$
$$J_{i\beta} = \frac{\pi}{2} F_{i\beta}(r_0)[f_i'(r_0) + b_\beta f_i(r_0)] . \tag{14}$$

The $N \times N$ reaction matrix is

$$\underline{K} = \underline{J}\,\underline{I}^{-1} , \tag{15}$$

and it is readily diagonalized,

$$K_{ij} = \sum_\alpha U_{i\alpha} \tan[\pi \mu_\alpha] (U^T)_{\alpha j} . \tag{16}$$

The eigenvector elements $U_{i\alpha}$ and eigenquantum defects μ_α are generally smooth energy-dependent parameters. They are utilized by MQDT to predict observables such as the photoionization cross section and the discrete en-

TABLE II. Two-electron basis functions used in the calculations.

Common basis for all calculations closed-type functions	Additional basis two-channel open-type functions	Additional basis five-channel open-type functions
$4s(4p\text{-}9p)$, $5s(5p\text{-}9p)$, $6s(6p\text{-}9p)$, $7s(7p\text{-}9p)$ $8s8p$, $8s9p$,	$4s(4p\text{-}6p)$	$4s(4p\text{-}6p)$
$3d(4p\text{-}9p)$, $4d(6p\text{-}8p)$, $5d(7p\text{-}8p)$, $6d8p$	$3d(4p\text{-}6p)$	$3d(4p\text{-}6p)$
$4p(5s\text{-}9s)$, $5p(6s\text{-}8s)$, $6p(7s\text{-}8s)$, $7p8s$		$4p(4s\text{-}6s)$
$4p(4d\text{-}8d)$, $5p(4d\text{-}8d)$, $6p(5d\text{-}8d)$, $7p(6d\text{-}8d)$ $8p7d$, $8p8d$		$4p(4d\text{-}6d)$
$3d(4f\text{-}9f)$, $4d(4f\text{-}8f)$, $5d(5f\text{-}8f)$, $6d(6f\text{-}8f)$ $7d(7f\text{-}8f)$,		$3d(4f\text{-}6f)$
$4f(5d\text{-}7d)$, $5f(6d\text{-}7d)$, $6f7d$		

ergy spectrum.[7,8,36] The energy-normalized K-matrix eigenchannels ψ_α having the same phase shift $\pi\mu_\alpha$ in each channel i are linear combinations of the unnormalized R-matrix eigenchannels ψ_β,

$$\psi_\alpha = \sum_\beta \psi_\beta (\underline{I}^{-1})_{\beta i} U_{i\alpha} \cos(\pi\mu_\alpha) \ . \tag{17}$$

At this point the standard techniques of multichannel quantum-defect theory are easily implemented on an arbitrarily fine energy mesh. It is only at this point that we distinguish between the open and weakly closed channels. To summarize, elimination of closed channels selects linear combinations of the ψ_α, namely, $\psi_\rho = \sum_\alpha \psi_\alpha A_{\alpha\rho}$, which decay exponentially at $r \to \infty$ in each closed channel ($i\varepsilon Q$) and which have the same eigenphase shift δ_ρ in each open ionization channel ($i\varepsilon P$). This elimination has the analytical structure[8]

$$\underline{\Gamma}' \underline{A} = \underline{\Lambda}' \underline{A} \tan\underline{\delta} \ , \tag{18}$$

where primes are introduced to avoid confusion with Eq. (3) and where

$$\Gamma'_{i\alpha} = \begin{cases} U_{i\alpha}\sin(\pi\nu_i + \pi\mu_\alpha), & i\varepsilon Q \\ U_{i\alpha}\sin(\pi\mu_\alpha), & i\varepsilon P \end{cases}$$
$$\Lambda'_{i\alpha} = \begin{cases} 0, & i\varepsilon Q \\ U_{i\alpha}\cos(\pi\mu_\alpha), & i\varepsilon P \ . \end{cases} \tag{19}$$

The number of nontrivial eigenvalues δ_ρ of this standard $N\times N$ eigensystem coincides with the number N_0 of channels that are open at the given energy E. Here $\nu_i = (-2\varepsilon_i)^{-1/2}$ is the effective quantum number in the ith closed channel. When all channels are closed, it is useful to solve Eq. (18) with the lowest channel *treated as though it were open anyway*. Then the single resulting eigenphase shift $\delta(E)/\pi$ is just the usual atomic quantum defect, and the nth discrete bound level $E^{(n)}$ is given by a Rydberg formula,

$$E^{(n)} = E_1 - \tfrac{1}{2}[n - \delta(E^{(n)})/\pi]^{-2} \ . \tag{20}$$

Lastly, computation of the photoabsorption strength involves also reduced electric dipole matrix elements connecting ψ_α to the $L=0$ ground state,

$$D_\alpha^{(L)} = \langle \Psi_\alpha \| r_1^{(1)} + r_2^{(1)} \| \Psi_0 \rangle \ . \tag{21}$$

Equation (21) is the dipole-length result. Its deviation from the dipole-velocity form gives a good measure of the inaccuracies in our variational wave functions,

$$D_\alpha^{(V)} = \langle \Psi_\alpha \| \nabla_1^{(1)} + \nabla_2^{(1)} \| \Psi_0 \rangle / \omega \ . \tag{22}$$

[Note that the derivatives used in this velocity form must act on the *true* wave functions without the extra factor $r_1 r_2$ mentioned after Eq. (6).] Finally the total photoionization cross section is given in a.u. by

$$\sigma = \frac{4\pi^2\omega}{3(137)} \sum_\rho |\, d_\rho \,|^2 \ , \tag{23}$$

where ω is the photon energy in a.u. and

$$d_\rho = \sum_\alpha D_\alpha A_{\alpha\rho} \ . \tag{24}$$

The ground-state energy and wave function are obtained by diagonalizing the Hamiltonian using a basis set of orbitals that vanish on the reaction surface. The energy level obtained is $E_{4s^2} = -0.6647$ a.u. which is lower than the experimental energy value[39] by 0.004 a.u. Because the calculated energy is too *low*, we know that the error is not caused by our truncation of the basis set nor by our restriction of the calculation to a finite volume. This discrepancy reflects an inadequacy of the model Hamiltonian used [Eq. (1)]. The major omission is the three-body dipole polarization term, which would be expected to have a positive expectation value in the calcium ground state of order $|\, \alpha_{cp}/r_1^2 r_2^2 \,|$. Using $r_1 \sim r_2 \sim 5$ a.u., this correction is of the same order of magnitude as our ground-state error. It becomes rapidly less important with increasing excitation, thus justifying its neglect in this study. To achieve higher accuracy than we find in this calculation, particularly for transition wavelengths, this is probably the element of our calculation which will be the most important to improve.

III. RESULTS AND COMPARISONS WITH EXPERIMENT

A. The discrete spectrum

Below $Ca^+(4s)$, all channels are closed and the energy spectrum is purely discrete. For $^1P^o$ and $^3P^o$ symmetries only two channels $4s\varepsilon p$ and $3d\varepsilon p$ are weakly closed, but basis functions in the strongly closed channels $4pns$ and $4pnd$ must be included to achieve reasonable agreement with experiment. The quantum defect δ/π derived from our two-channel calculation [as discussed above Eq. (20)] is compared with experimental[39] calcium quantum defects in Fig. 1. The agreement is generally quite good. The energy dependence of δ/π in particular is faithfully reproduced, with a small discrepancy visible at the $4s$ threshold ($\nu_{3d} = 2.832$). The rise of δ/π by roughly one unit is associated with the $3d4p$ perturbing configuration; the much faster rise for $^3P^o$ than for $^1P^o$ reflects the stronger $4s\varepsilon p$-$3d\varepsilon p$ channel interactions expected for $^1P^o$. Figure 1 also shows as dashed lines the values of δ/π predicted by a two-channel MQDT fit using energy-independent short-range parameters.[25] The better agreement of our calculated δ/π with experiment confirms that the energy dependence of $U_{i\alpha}$ and μ_α is important and is correctly predicted by theory. Figure 2 shows our two-channel $^1P^o$ parameters μ_1, μ_2, and θ as functions of the energy. The assumption that these parameters are constant is seen to be quantitatively valid over an energy range of at most 0.03 a.u. near the $4s$ threshold. Figure 2 also confirms the trend toward zero channel mixing at low energies that has been observed in previous studies of this type.[3,4,15,30,31]

The characteristic energy dependence at low energies is familiar, but Fig. 2 also shows a new effect not seen in the Be or Mg calculations. At higher energies, $\varepsilon_{4s} \gtrsim 0.02$ a.u., the two-channel MQDT parameters acquire a strong energy dependence yet again. This directly reflects the influence of virtual excitations into the $4pns$ channel, which are just beginning to become energetical-

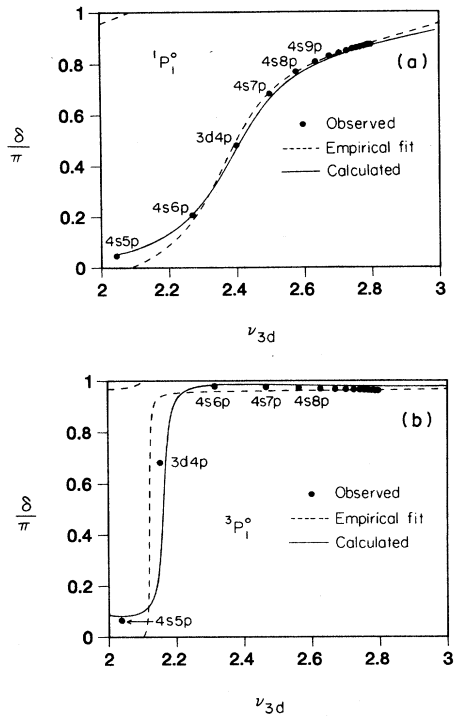

FIG. 1. Calculated and observed Lu-Fano plot for calcium $^1P^o$ (a) and $^3P^o$ (b) discrete levels below the $Ca^+(4s)$ threshold. The solid circles are data obtained from Ref. 39, the dashed curve is the empirical quantum defect results of Ref. 25, and the solid curve is the present R-matrix calculation. The ordinate is the quantum defect in the $4s$ channel, while the abscissa is the effective quantum number in the $3d$ channel.

ly allowed. Moores[42] attempted years ago to predict the photoionization cross section by extrapolating two-channel parameters obtained empirically at $\varepsilon_{4s}<0$. The poor results obtained by Moores' analysis are easily understood in view of the strong energy dependence in Fig. 2 which he neglected. Figure 3 shows the relevant $^1P^o$ hyperspherical potential curves for calcium which were

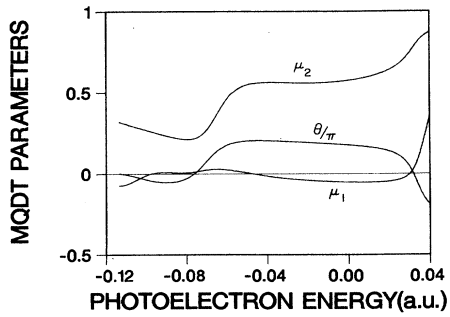

FIG. 2. Two-channel $^1P^o$ mixing parameters of quantum-defect theory are shown for calcium as a function of the photoelectron energy in the lowest channel, ε_{4s}. The μ_α are related to the eigenvalues of the reaction matrix, while θ is the rotation angle needed to diagonalize this matrix.

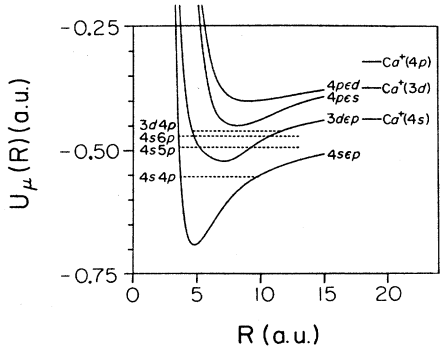

FIG. 3. Adiabatic potential curves for $^1P^o$ calcium are shown as a function of the hyperspherical radius. (From Ref. 14.)

obtained in Ref. 2. From these results, virtual excitations into the $4pns$ channel were predicted[14] to become important near the minimum of the $4p\varepsilon s$ adiabatic potential curve, which lies slightly below the $4s$ threshold. This conclusion is verified qualitatively by the present calculation, although the present energy dependence begins at a somewhat higher energy than was expected on the basis of Fig. 3.

Another coupled-channel calculation of the $L=1$ MQDT channel-mixing parameters for calcium was published by Pandey, Jha, and Armstrong.[43] Their two-channel results at the $4s$ threshold agree reasonably well with experiment and with our calculation. In our study the strongly closed channel functions $4pns$ and $4pnd$ are very important, but they appear to have been neglected by Ref. 43. Without them, in fact, we find the eigenquantum defects at the $4s$ threshold to be too low by more than 0.1. Reference 43 also makes a severe local approximation to the integral-exchange term in the course of solving the close-coupled integro-differential equations.

B. Resonances in the photoionization continuum

The energy region between the $4s$ and $3d$ thresholds has been studied extensively, both experimentally and theoretically. The best experimental results seem to be those of Newsom,[9] obtained with higher resolution than the recent synchrotron measurement of Karamatskos *et al.*[12] The absolute normalization of Newsom's observed photoionization cross section is apparently too low by a factor of about 5, and has been renormalized to achieve agreement with the absolute measurement at one wavelength by McIlrath and Sandeman.[10] The renormalized experimental results of Newsom are compared with our R-matrix calculation in Fig. 4. The agreement is generally quite good, with the calculated $3d5p$ resonance (at $\varepsilon_{4s}\sim 0.018$) slightly too low and the narrow $3d6p$ resonance (at $\varepsilon_{4s}\sim 0.033$) over a factor of 2 too low. Note the exceptional agreement in Fig. 4 between length and velocity results for the cross section. Again, the inclusion of several strongly closed orbitals such as $5s5p$ proved to be quite important in reducing the difference

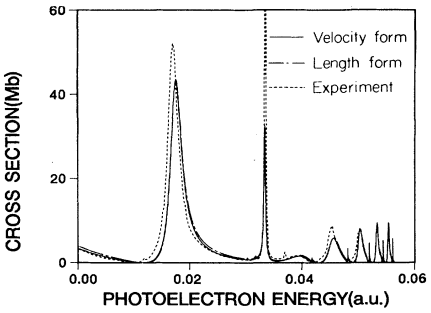

FIG. 4. Length and velocity results for the total photoionization cross section of calcium are compared with the experimental results of Newsom (Ref. 9), after rescaling by the overall factor suggested by McIlrath and Sandeman (Ref. 10). The energy range shown is between the $Ca^+(4s)$ and $Ca^+(3d)$ thresholds.

between length and velocity to the level shown. These results represent a substantial improvement over previous calculations,[1,2] especially in the vicinity of the $4p5s$ resonance (at $\varepsilon_{4s} \sim 0.04$ a.u.).

The theoretical calculation shown in Fig. 4 includes two channels below $\varepsilon_{4s} \sim 0.014$, a.u., and five channels ($4s\varepsilon p$, $3d\varepsilon p$, $3d\varepsilon f$, $4p\varepsilon s$, $4p\varepsilon d$) at all higher energies. In fact, the two-channel calculation gives results close to the five-channel calculation over the entire energy range of Fig. 4. Note that the two-channel calculation is only accurate to the extent that strongly closed channel resonances like $4p5s$ are confined entirely within the reaction volume. For the two-channel calculation using an R-matrix boundary at $r_0 = 14$ a.u., discrepancies with the five-channel treatment becomes significant above $\varepsilon_{4s} \sim 0.03$ a.u. The agreement is greatly improved by increasing r_0 to 18 a.u. and slightly more by using $r_0 = 22$ a.u. in the two-channel treatment. The five-channel results are far less sensitive to the choice of r_0, since $4pns$, $4pnd$, and $3dnf$ excitations are no longer *assumed* to be confined within the reaction volume. All two-channel and five-channel results shown here were obtained using $r_0 = 18$. The agreement between these alternative ways of performing the R-matrix calculation gives a powerful check on its validity, and points to its extensive flexibility.

The very different observed and calculated peak heights for the $3d6p$ resonance seem to signal a serious problem with our treatment. In fact, an interesting cancellation effect occurs at an energy very close to this autoionizing level that greatly magnifies any small errors in the calculation. In a strictly two-channel system, of course, the height of successive autoionizing levels is nearly independent of n while their widths decrease smoothly and monotonically as n^{-3}. The nonmonotonic variation of widths from one level to the next in Fig. 4 thus reflects the influence of the closed $4p\varepsilon s$ channel which is just becoming energetically accessible. The presence of this channel causes the energy dependence of the two-channel ($4s\varepsilon p$-$3d\varepsilon p$) MQDT parameters above $\varepsilon_{4s} = 0.02$ a.u. In particular the mixing angle vanishes at $\varepsilon_{4s} = 0.032$, implying that there is *no mixing between $4s\varepsilon p$ and $3d\varepsilon p$ at this particular energy.* If an autoionizing level were present at exactly this energy, it would in fact be a true bound state (i.e., its decay width would vanish). Our difficulty in reproducing the exact experimental height and width of $3d6p$ derives mostly from the fact that it lies very close to the energy at which the channel mixing disappears. The photoionization cross section in the vicinity of this state is then unusually sensitive to error in its height and width, although its integrated strength is probably described accurately. The destructive interference occurring at $\varepsilon_{4s} = 0.032$ a.u. is a simple example of cancellation between amplitudes for two alternative and indistinguishable decay pathways,

$$3dnp \rightarrow 4s\varepsilon p$$
and (25)
$$3dnp \rightarrow 4pns \rightarrow 4s\varepsilon p \ .$$

This interpretation was suggested by Altun *et al.*[1] It will be further documented in Sec. III D by studying the probability densities directly.

Figure 5 compares experimental and theoretical photoionization cross sections at higher energies still, between the $3d$ and $4p$ thresholds. The absolute normalization of the experimental cross section was not obtained by Connerade *et al.*,[11] so we have normalized the experimental curve to give the best overall agreement with our velocity calculation. Agreement between theory and experiment is somewhat inferior to that found at lower energies, but it is still superior to that obtained by Scott *et al.*[2] or by Altun *et al.*[1] Dipole length and velocity results are again very close in Fig. 5, but their difference is somewhat larger than we found at lower energies. The $4pns$ and $4pnd$ resonances responsible for the quasiperiodic autoionization structures in Fig. 5 are so broad and intermixed that we have not assigned quantum numbers to specific features. One mild surprise to us was the very great importance of the $3d\varepsilon f$ channel in this calculation. If it is omitted, the $4pnd$ resonances become much narrower and the spectrum is severely distorted. In retrospect this seems reasonable, however, considering that the outermost nd electron *tends to gain both energy and angular momentum in the course of its*

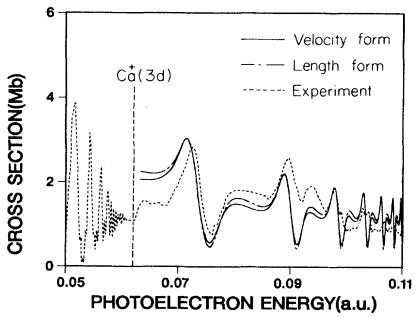

FIG. 5. Total photoionization cross section for calcium is shown as a function of ε_{4s} at higher energies, between the $3d$ and $4p$ thresholds. The present calculation is compared with the relative experimental cross section obtained by Connerade *et al.* (Ref. 11).

autoionization. The dominance of the $4pnd \rightarrow 3d\varepsilon f$ decay channel over the $4pnd \rightarrow 3d\varepsilon p$ channel is confirmed by examining the electron-ion scattering matrix in the following section. (See also Fig. 8 of Ref. 2.)

C. Evolution of channel interactions with increasing energy

The agreement between calculated and experimental results suggests that we have an excellent description of calcium channel interactions. Accordingly we attempt in the following to outline a more qualitative, global view. To begin with, our primary aim is to understand the *smooth* channel-mixing parameters such as the reaction matrix K. These do not reflect any resonance effects associated with closed channels, and therefore can be given the simplest interpretation. The reaction matrix often possesses poles, however, which makes it preferable to work instead with the equivalent quantum-defect matrix $\underline{\mu}=\pi^{-1}\tan^{-1}(\underline{K})$. Denoting the eigenvectors and eigenvalues of $\underline{K}$ by $U_{i\alpha}$ and $\tan(\pi\mu_\alpha)$, the elements of the matrix μ_{ij} are given by

$$\mu_{ij}=\sum_\alpha U_{i\alpha}\mu_\alpha(\underline{U}^T)_{\alpha j} \ . \tag{26}$$

(The μ_α should not be confused with this real symmetric matrix μ_{ij}, representing, in fact, its eigenvalues.) This matrix tends to be smoother than either K_{ij} or the equivalent $U_{i\alpha}$ and μ_α, and is better suited for interpolation. Table III gives the calculated $^1P^o$ quantum-defect matrix and the associated reduced dipole-matrix elements, related to these defined in Eqs. (21) and (22) by $d_i^{(L,V)}=\sum_\alpha U_{i\alpha}D_\alpha^{(L,V)}$. This table should provide sufficient information to reproduce most of our results in Figs. 4 and 5.

In any case, the channel-interaction matrix having the simplest *physical interpretation* is undoubtedly the short-range scattering matrix,

$$S_{ij}\equiv\sum_\alpha U_{i\alpha}\exp(2i\pi\mu_\alpha)(\underline{U}^T)_{\alpha j} \ . \tag{27}$$

This is just the quantum-mechanical amplitude that an electron which collides with the target ion (Ca^+) in channel j will recoil from the ion in channel i. Because $\underline{S}$ is constructed from $\underline{K}$ and does not incorporate any boundary conditions at $r\rightarrow\infty$, it remains a smooth function of energy like $\underline{\mu}$, devoid of all resonance effects. It should be remembered, however, that this is not the physical scattering matrix which can connect open channels only, and which displays resonance effects associated with closed channels.

Figure 6 shows the absolute squares of several elements of the five-channel short-range scattering matrix as functions of energy. Note in particular the very strong ($\sim$60%) mixing between $4p\varepsilon d$ and $3d\varepsilon f$. It is far stronger than the $4p\varepsilon d$-$3d\varepsilon p$ mixing, as surmised in Sec. II B above, and reflects the very large width of the $4pnd$ autoionizing resonances. In fact, the mixing between these channels is strong enough to be reminiscent of the + or − states in helium and beryllium.[14] Two eigenchannels of the calcium atom apparently have this same basic structure, $4p\varepsilon d\pm 3d\varepsilon f$.

Also given in Fig. 6 is the squared $4s\varepsilon p$-$3d\varepsilon p$ element

TABLE III. Quantum-defect matrices and reduced dipole matrix elements, as defined by Eq. (26) and the ensuing discussion.

μ_{ij}				
$4s\varepsilon p$	$3d\varepsilon p$	$3d\varepsilon f$	$4p\varepsilon s$	$4p\varepsilon d$
		(a) At the $Ca^+(3d)$ threshold		
−0.0217	0.0546	0.0761	−0.1486	−0.1187
0.0546	−0.1205	0.0962	−0.2373	−0.0734
0.0761	0.0962	−0.0639	−0.0627	0.1988
−0.1486	−0.2373	−0.0627	−0.0779	0.2339
−0.1187	−0.0734	0.1988	0.2399	−0.0592
		Dipole length matrix elements $d_i^{(L)}$		
−0.1039	−0.3183	0.3519	−0.7986	−0.2040
		Dipole velocity matrix elements $d_i^{(V)}$		
−0.0140	−0.3413	0.3429	−0.7822	−0.1500
		(b) At the $Ca^+(4p)$ threshold		
−0.0384	0.0639	0.0545	−0.1687	−0.0655
0.0639	−0.1487	0.0861	−0.2508	−0.0483
0.0545	0.0861	−0.0681	−0.0524	0.1500
−0.1687	−0.2508	−0.0524	−0.0731	0.1688
−0.0665	−0.0483	0.1500	0.1688	−0.0509
		Dipole length matrix elements $d_i^{(L)}$		
0.1290	−0.1318	0.2086	−0.5440	−0.0424
		Dipole velocity matrix elements $d_i^{(V)}$		
0.1925	−0.1697	0.2023	−0.5145	−0.0025

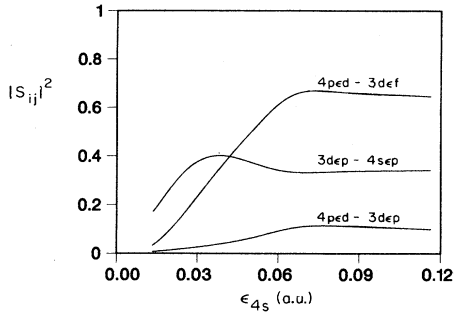

FIG. 6. Absolute squares of selected elements of the short-range scattering matrix are shown as functions of the photoelectron energy between the 4*s* and 4*p* thresholds.

of the short-range scattering matrix. This interaction parameter is in the range $\sim 30\%$ over most of the energy range shown. It is quite different from zero everywhere, in distinct contrast to the corresponding element of the two-channel problem considered in Sec. III B above. [In a two-channel system the off-diagonal squared element is $|S_{12}|^2=\sin^2(2\theta)\sin^2[\pi(\mu_2-\mu_1)]$.] Since θ goes through zero in Fig. 2 between the 4*s* and 3*d* thresholds, $|S_{12}|^2$ vanishes at that point also. This may seem to contradict the five-channel results in Fig. 6, but it does not. In the two-channel calculation, higher channels such as $4p\varepsilon s$ are treated as strongly closed, meaning that their low-lying resonances which are confined within the reaction zone are incorporated. The five-channel study instead treats $4p\varepsilon s$ as though it were open and so the 4*p*5*s* resonance in particular does not show up in $\underline{S}$. Thus when interpreting channel-interaction strengths it is essential to keep in mind which channels are treated as open, and also which strongly closed channels are included. This confirms the interpretation given in Sec. III B that the vanishing of the $3d\varepsilon p$-$4s\varepsilon p$ interaction at one energy derives from destructive interference between the direct amplitude and the $3d\varepsilon p$-4*pns*-$4s\varepsilon p$ amplitude.

D. Probability density plots

A great deal can be deduced from the wave functions themselves, although they contain so much information that it is nontrivial to extract the major features. We focus here on components of the *radial* probability density because radial correlations are normally more important than angular correlations in determining channel-interaction strengths. One way of displaying this information is to plot $\langle|\psi_\alpha|^2\rangle$ as a function of (r_1,r_2) after integrating over the four angular degrees of freedom. The αth independent solution can be decomposed into its various partial-wave components according to

$$\psi_\alpha=\sum_{l_1 l_2} g_\alpha^{l_1 l_2}(r_1,r_2)Y_{l_1 l_2 LM}(\Omega_1,\Omega_2)\ . \tag{28}$$

In this notation the total angle-averaged density takes the form

$$\langle|\psi_\alpha|^2\rangle=|g_\alpha^{sp}(r_1,r_2)|^2+|g_\alpha^{ps}(r_1,r_2)|^2 + |g_\alpha^{pd}(r_1,r_2)|^2+\ldots\ . \tag{29}$$

In the case of $^1P^o$ states of Be and Mg studied in Fig. 3 of Ref. 15, angular correlations play a negligible role and the first term $|g^{sp}|^2$ dominates. In calcium, however, the channel interaction of greatest interest at low energies is $4s\varepsilon p$-$3d\varepsilon p$, and accordingly both $|g_\alpha^{sp}|^2$ and $|g_\alpha^{pd}|^2$ must be shown for each independent solution ψ_α. [Note that the Pauli principle ensures that $|g_\alpha^{sp}(r_1,r_2)|^2=|g_\alpha^{ps}(r_2,r_1)|^2$, permitting us to focus on the terms with $l_1\le l_2$ without losing any information.]

Figure 7 shows these components of the $^1P^o$ probability density inside the reaction zone, obtained from the two-channel variational calculation. The densities involve two three-dimensional plots (*sp* and *pd*) for each ψ_α, and there are two independent solutions ψ_α at each energy. Rather than labeling the horizontal axes in Fig. 7 by (r_1,r_2) we have simply indicated the channel involved. It should be remembered, though, that the horizontal axes in Fig. 7 are (r_1,r_2) and that each radial coordinate ranges from 0 to 18 a.u. Remember as well that the 4*pns* and 4*pnd* channels only include trial orbitals which vanish at $r=r_0$, which do not permit the outermost electron to escape the reaction zone. This electron can escape the reaction zone only in the channels $4s\varepsilon p$ and $3d\varepsilon p$. Note also that the *sp* and *pd* densities have the same vertical scale, so that the relative amount of density in the two plots for a given state α provides an index of the strength of angular correlations.

At the lowest energy $\varepsilon_{4s}=-0.114$ a.u., the two-channel MQDT parameters of Fig. 2 show essentially no mixing of $4s\varepsilon p$ and $3d\varepsilon p$. This negligible mixing is also apparent in Fig. 7(a), with the $\alpha=1$ wave function mainly localized in the $4s\varepsilon p$ potential valley of the (r_1,r_2) plane. A non-negligible contribution to the $\alpha=1$ density is contributed by the $3d\varepsilon p$ channel, but it looks in fact artificially large here because of the exponential growth near $r_2\sim r_0$. (Physical boundary conditions at $r\to\infty$, such as the finiteness of ψ_α in that limit, have not been imposed at this point. They are imposed later by superposing the ψ_α as is usual in quantum-defect theory.) The second independent solution $\alpha=2$ in Fig. 7(a) shows purely exponential growth (chopped off in the plot) in the $3d\varepsilon p$ channel, with negligible amplitude apparent in the $4s\varepsilon p$ channel.

A higher energy is shown in Fig. 7(b), right at the 4*s* threshold. Here the $4s\varepsilon p$-$3d\varepsilon p$ mixing is much stronger than that in Fig. 7(a). Over half of the $\alpha=1$ density is in the $4s\varepsilon p$ potential valley, but not much more than half. Similarly the $\alpha=2$ eigenstate has somewhat more of its density in the $3d\varepsilon p$ valley, but it shows a sizable contribution from the $4s\varepsilon p$ channel. At this energy there is still no visible amplitude in either of the strongly closed channels 4*pns* and 4*pnd*, but excitations into 4*pns* begin at just slightly higher energies. (See Fig. 3.)

The next highest energy $\varepsilon_{4s}=0.032$, shown in Fig. 7(c), is the energy at which the $4s\varepsilon p$-$3d\varepsilon p$ channel-mixing angle θ vanishes in Fig. 2. Note how the $\alpha=1$ density shows no $3d\varepsilon p$ component at $r_2\to r_0$, while the $\alpha=2$ density shows no $4s\varepsilon p$ component. On the other

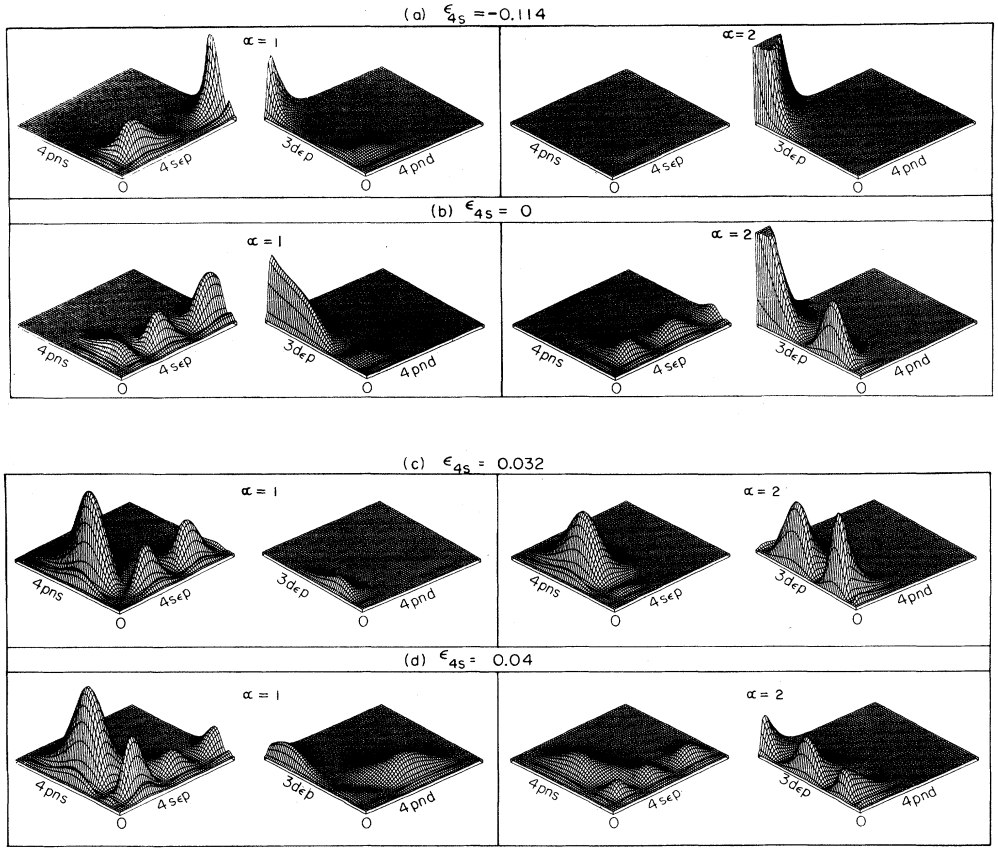

FIG. 7. Radial *sp* and *pd* components of the $^1P^o$ probability density are shown as functions of (r_1, r_2). The radial axes range between 0 and 18 a.u., though these labels have been suppressed for clarity, with the relevant channel indicated instead. Two plots are shown for each of the four energies, corresponding to the two eigenchannels ψ_α obtained in our two-channel calculation. Note the general increase of channel-interaction strength with increasing energy.

hand, both $\alpha = 1$ and 2 now show a dominant contribution from the closed $4pns$ channel. The energy is sufficiently high at this point to excite $4p5s$, the lowest quasi-bound-state in this channel. Note that this state just barely fits within our reaction volume of radius $r_0 = 18$ a.u. It is the presence of this new excitation mode which permits a destructive interference to develop between the two decay pathways shown in Eq. (25), a phenomenon that requires at least three channels to be involved. At this energy $\varepsilon_{4s} = 0.032$ a.u., the closed $4pnd$ channel still plays no significant role in the dynamics.

Finally, Fig. 7(d) shows the densities at an energy $\varepsilon_{4s} = 0.04$ a.u., still substantially below the $3d$ threshold. At this energy there is no longer any destructive interference between the two decay pathways of Eq. (25). This shows up in Fig. 7(d) where the densities within the $4s\varepsilon p$ and $3d\varepsilon p$ valleys are comparably excited—implying strong channel mixing—in both the $\alpha = 1$ and 2 independent solutions. The $4pns$ channel still plays a major role in the dynamics. In Fig. 7(d) for the first time the energy has increased enough to excite the lowest mode in the $4pnd$ potential valley, which would carry the independent-electron designation $4p4d$. At even higher energies than are shown in Fig. 7, the interactions between all channels remain strong. Another channel $3d\varepsilon f$ becomes important as well.

These plots thus help to document the general tendency for higher channels to become excited as the energy is increased. This alone is a fairly obvious property of any many-particle system. What is less obvious about these results is that the energies at which successive channels become important correlate nicely with the hyperspherical potential curves of Fig. 3.

IV. DISCUSSION

The present study of calcium and the parallel treatment of strontium by Aymar *et al.*[17] have both demonstrated that a good theoretical description can be obtained for the heavier alkaline-earth metals, despite extremely strong correlations between the outer electrons and despite very sensitive centrifugal barrier effects. These calculations treat the atom in *LS* coupling, which breaks down near spin-orbit-split thresholds. In those regions of the spectrum a geometrical frame transformation permits *jj*-coupled reaction matrices to be obtained from the *LS*-coupled matrices. Spin-orbit effects at this level will be considered in a separate article.[44] For barium and radium these spin-orbit effects are much more important, and they must also be considered *within* the

reaction zone as in Ref. 29.

All of the alkaline-earth metals share the unusually strong channel coupling seen above for calcium. Autoionization rates of the lower-lying doubly excited states are nearly 2 orders of magnitude faster than the corresponding states of helium. In fact, an equally strong channel coupling is present in helium, as in the + or − identified by Cooper *et al.*[45] But the degeneracy of $He^+(nl)$ thresholds prevents this strong channel coupling from being manifested as a large autoionization width as in Be, Mg, Ca, Sr, Ba, and Ra.[14] Still, within the reaction zone, the channel interactions overwhelm the small intrashell energy splittings of each alkaline-earth ion. At small distances, accordingly, the wave functions and channel interaction strengths look remarkably similar for all of these atoms including helium.

The present calculations are far from saturating a minicomputer having the capacity of a VAX or RIDGE computer. In fact, all calculations shown in this paper require about two hours on such a small machine, or nearly twenty minutes on an IBM 3084. By including many more channels and a substantially larger reaction volume, it now seems plausible to try a similar calculation for the low-lying Wannier ridge states (e.g., such as $8s8p$ in calcium). On the other hand, considering the inefficiency of coupled-channel expansions at high energies, the development of a new analytical framework to deal with that portion of the spectrum is becoming increasingly important.

ACKNOWLEDGMENTS

This work was supported in part by the National Science Foundation. One of us (C.H.G.) also received support from the Alfred P. Sloan Foundation.

[1]Z. Altun, S. L. Carter, and H. P. Kelly, J. Phys. B **15**, L709 (1982); also Phys. Rev. A **27**, 1943 (1983).
[2]P. Scott, A. E. Kingston, and A. Hibbert, J. Phys. B **16**, 3945 (1983).
[3]C. H. Greene, Phys. Rev. A **28**, 2209 (1983); *ibid.* **32**, 1880 (1985); for a recent review see C. H. Greene, J. Opt. Soc. Am. B **4**, 775 (1987).
[4]H. Le Rouzo and G. Raseev, Phys. Rev. A **29**, 1214 (1984).
[5]U. Fano and C. M. Lee, Phys. Rev. Lett. **31**, 1573 (1973).
[6]M. J. Seaton, Rep. Prog. Phys. **46**, 97 (1983).
[7]U. Fano and A. R. P. Rau, *Atomic Collisions and Spectra* (Academic, Orlando, 1986).
[8]C. H. Greene and Ch. Jungen, Adv. At. Mol. Phys. **21**, 51 (1985).
[9]G. H. Newsom, Proc. Phys. Soc. London **87**, 975 (1966). [This experiment has been analyzed using MQDT by K. Ueda, Phys. Rev. A **35**, 2484 (1987).]
[10]T. J. McIlrath and R. J. Sandeman, J. Phys. B **5**, L217 (1972).
[11]J. P. Connerade, M. A. Baig, W. R. S. Garton, and G. H. Newsom, Proc. R. Soc. London, Ser. A **371**, 295 (1980).
[12]N. Karamatskos, M. Mueller, M. Schmidt, and P. Zimmermann, J. Phys. B **18**, L107 (1985).
[13]J. Dubau and J. Wells, J. Phys. B **6**, 1452 (1973); G. N. Bates and P. L. Altick, *ibid.* **6**, 653 (1973); V. Radojevic and W. R. Johnson, Phys. Rev. A **31**, 2991 (1985).
[14]C. H. Greene, Phys. Rev. A **23**, 661 (1981).
[15]P. F. O'Mahony and C. H. Greene, Phys. Rev. A **31**, 250 (1985).
[16]U. Fano and L. Fano, *Physics of Atoms and Molecules* (University of Chicago Press, Chicago, 1972), p. 310.
[17]M. Aymar, E. Luc-Koenig, and S. Watanabe, J. Phys. B (to be published).
[18]T. F. Gallgaher, W. Sandner, and K. A. Safinya, Phys. Rev. A **23**, 2969 (1981); W. Sandner, K. A. Safinya, and T. F. Gallagher, *ibid.* **24**, 1647 (1981); R. Kachru, N. H. Tran, P. Pillet, and T. F. Gallagher, *ibid.* **31**, 218 (1985).
[19]R. R. Freeman, J. Bokor, and W. E. Cooke, Phys. Rev. A **21**, 148 (1980); L. A. Bloomfield, R. R. Freeman, W. E. Cooke, and J. Bokor, Phys. Rev. Lett. **53**, 2234 (1984).
[20]O. C. Mullins, J. E. Hunter III, J. S. Keller, and R. S. Berry, Phys. Rev. Lett. **54**, 410 (1985).
[21]E. Matthias, P. Zoller, D. S. Elliot, N. D. Pilch, S. J. Smith, and G. Leuchs, Phys. Rev. Lett. **50**, 1914 (1983).
[22]O. C. Mullins, Y. Zhu, and T. F. Gallagher, Phys. Rev. A **32**, 243 (1985); O. C. Mullins, Y. Zhu, E. Y. Xu, and T. F. Gallagher, Phys. Rev. A **32**, 2234 (1985).
[23]M. Aymar, Phys. Rep. **110**, 163 (1984).
[24]J. A. Armstrong, J. J. Wynne, and P. Esherick, J. Opt. Soc. Am. **69**, 211 (1979); J. A. Armstrong, P. Esherick, and J. J. Wynne, Phys. Rev. A **15**, 180 (1977).
[25]J. J. Wynne and J. A. Armstrong, Comments At. Mol. Phys. **8**, 155 (1979).
[26]D. A. Harmin, Phys. Rev. A **24**, 1491 (1981); *ibid.* **26**, 2656 (1982); Phys. Rev. Lett. **49**, 128 (1982).
[27]K. T. Lu and A. R. P. Rau, Phys. Rev. A **28**, 2623 (1983); P. F. O'Mahony and K. T. Taylor, Phys. Rev. Lett. **57**, 2931 (1986).
[28]K. Ueda, J. Quant. Spectrosc. Radiat. Transfer **33**, 77 (1985); E. de Prunele, Phys. Rev. A **35**, 496 (1987); Ning Yi Du and C. H. Greene, *ibid.* **36**, 971 (1987).
[29]K. Bartschat, M. R. H. Rudge, and P. Scott, J. Phys. B **19**, 2469 (1986).
[30]P. F. O'Mahony and S. Watanabe, J. Phys. B **18**, L239 (1985).
[31]P. F. O'Mahony, Phys. Rev. A **32**, 908 (1985).
[32]P. G. Burke and K. T. Taylor, J. Phys. B **8**, 2620 (1975); P. G. Burke and D. Robb, Adv. At. Mol. Phys. **11**, 143 (1975).
[33]W. Kohn, Phys. Rev. **74**, 1763 (1948).
[34]J. Callaway, Phys. Rep. **45**, 89 (1978).
[35]R. K. Nesbet, *Variational Methods in Electron-Atom Scattering Theory* (Plenum, New York, 1980), Chap. 2.
[36]D. Dill and U. Fano, Phys. Rev. Lett. **29**, 1203 (1972); C. M. Lee, Phys. Rev. A **10**, 1598 (1974); C. H. Greene and R. N. Zare, *ibid.* **25**, 2031 (1982).
[37]J. P. Desclaux, Comput. Phys. Commun. **1**, 216 (1969).
[38]W. Kohn and L. S. Sham, Phys. Rev. **140**, A1133 (1965).
[39]J. Sugar and C. Corliss, J. Phys. Chem. Ref. Data **8**, 865 (1979).
[40]See, e.g., C. Froese Fischer, *The Hartree-Fock Method for Atoms* (Wiley, New York, 1977).
[41]See, e.g., M. J. Seaton, Comput. Phys. Commun. **25**, 87

(1982).
[42]D. L. Moores, Proc. Phys. Soc. London **88**, 843 (1966).
[43]K. C. Pandey, S. S. Jha, and J. A. Armstrong, Phys. Rev. Lett. **44**, 1583 (1980); J. A. Armstrong, S. S. Jha, and K. C. Pandey, Phys. Rev. A **23**, 2761 (1981).
[44]L. Kim and C. H. Greene, Phys. Rev. A (to be published).
[45]J. W. Cooper, U. Fano, and F. Prats, Phys. Rev. Lett. **10**, 518 (1963).